RSC Advances

ROYAL SOCIETY OF CHEMISTRY

www.rsc.org/advances

High performances bipolar spin filtering and switching functions of poly-(terphenylene-butadiynylene)s between zigzag graphene nanoribbon electrodes

Dan Zhang[a], Mengqiu Long[a,b,*], Xiaojiao Zhang[c], and Hui Xu[a,*]

[a]*Institute of Super-microstructure and Ultrafast Process in Advanced Materials, School of Physics and Electronics, Central South University, Changsha 410083, China*

[b]*Department of Physics and Materials Science, City University of Hong Kong, Hong Kong, China*

[c]*Physical Science and Technology College of Yichun University, Yichun 336000, China*

Abstract: Using the nonequilibrium Green's function method combined with spin-polarized density functional theory, we investigate the spin-resolved electronic transport properties of the device about poly-(terphenylene-butadiynylene)s (PTBs) between two symmetric ferromagnetic zigzag graphene nanoribbon (ZGNR) electrodes. The bipolar spin filtering effect, rectifying, and negative differential resistance have been found. More interestingly, the on/off ratio of order 10^7 is also predicted by changing the angle between the PTB and ZGNR electrodes planes. Further analyses show that the matching of electronic wave functions among both electrodes and the PTB plays a key role in the multi-functions of the PTB based devices. And the coupling between the alkyne triple bond and phenyl ring of PTBs is critical to the value of the spin-resolved current and the on/off ratio. These phenomena suggest the proposed PTBs based devices have a potential utilization in molecular spin diode and molecular switch.

Keywords: poly-(terphenylene-butadiynylene)s, zigzag graphene nanoribbons, electronic transport property, bipolar spin-filtering effect, switching function

* Corresponding authors.
E-mail addresses: mqlong@csu.edu.cn (M. Q. Long), cmpxhg@csu.edu.cn (H. Xu).

Introduction

The traditional semi-conductive electronic devices have been confronted with unprecedented challenge[1,2], following the molecular electronic devices attract many people's attention, and tremendous efforts have been devoting to them both experimentally[3,4] and theoretically[5-7]. Lots of interesting phenomena have been found, including spin-valve[8], spin filtering[9], spin crossover[10], negative differential resistance (NDR)[11], switching effect[12,13], rectification[14], and so on. The electronic transport properties of molecular devices not only dependent on the structure of the molecular, but also have a huge relationship with the properties of both electrodes. Thus, the choice of the electrodes is very important in device designing. Generally, the metallic electrode is one of the most popular ones, and the molecular connect with the metallic electrodes by thiol (-SH) group. Nevertheless, it is not an ideal choice in view of electrical transparency, mechanical stability and atomic level control over the bonding geometry[15-17].

The discovery and successful preparation of graphene [18] and graphene nanoribbons (GNRs)[19,20] bring a new revolution to the molecular devices due to their remarkable electronic properties[21], high electronic mobility[22], long spin relaxation times and lengths[23], weak spin-orbital coupling effect[24], gate tunability[25] and so on. Especially, lots of researches are concentrating on zigzag graphene nanoribbons (ZGNRs) for its edge magnetism and unique transport properties[26-28]. Jin, and Rong, *et al.*[29,30] have realized the C chains between GNRs in experiment. And then Dong, *et al.*[31] reported their theoretical results for the C chain between transversely symmetric GNRs electrodes, and perfect spin-filtering effect couples with spin rectification ratio of order 10^6 have been found. Li, *et al.*[32] found the oligo(p-phenylene-vinylene) (OPV) molecule without or with different side groups between two ZGNR electrodes can realize the NDR and rectifying effects. What's more, the changing of OPV conformations respect to ZGNRs can take great changes to the spin transport properties[33]. All these researches show that the spin-filtering, switching, and NDR *et al.* could be coexisted in a device, which suggests the multi-functional and high

performance molecular devices have been a tendency in future.

In 2014, Cirera, *et al.* [34] successfully synthesized the extended poly-(terphenylene-butadiynylene)s (PTBs) $\left[-C\equiv C-Ph_3-C\equiv C-\right]_n$ by vicinal surface templating. The PTBs is rich in triple and double bonds of C atoms, which can be formed π bonds and benefit for the electrons' conductive. Theoretical calculations show it is a semi-conductor with a direct band gap of 1.6 eV[34], which indicates it has a potential utilization in organic molecular devices. However, the electronic transport properties of PTBs devices have not been reported. In this letter, we are mainly probing the spin transport properties of PTBs based device. Considering the contact between PTBs and the electrodes, meanwhile to realize multi-functional device, we choose symmetric ferromagnetic ZGNRs as both left and right electrodes. Our calculations show the bipolar spin-filtering effect, NDR, rectifying, and switching functions can be realized. More importantly, the spin-filtering efficiency is 100%, the rectifying can reach 6.8×10^3 and the on/off ratio is as high as 10^7.

Models and methods

The structure of the PTBs is shown in Fig. 1(a), and the structure in the red dashed rectangle is the unit cell. We build the two probe system of M1 by connecting the PTB unit cell with two symmetric ZGNRs of 6 ribbon width (6ZGNRs) within the same plane (i.e. *y*-*z* plane), as shown in Fig. 1(b). The blue shade areas are the electrode regions. Former researches have pointed out that the rotating of phenyl rings can be realized by many methods, such as scanning tunneling microscopy manipulation[35], laser pulses[36], mechanical operation[37], adding electric field[38], and so on. Therefore, we get the three other devices by rotating the PTB plane around the C chain (*z* axis) and make the angle between PTB plane and both the 6ZGNRs electrodes plane changes from 0° to 30°, 60° and 90°, respectively, which are marked as M2, M3 and M4 for short. In the two-probe system, the spin orientation of the left (right) electrode can be controlled by an external magnetic field[39,40], which plays an important role in spin devices[41]. Here, the edges of the electrode 6ZGNRs are assigned in ferromagnetic state, which show metallic properties[42,43]. And two kinds of

spin orientation between the left and right electrodes have been considered: parallel configuration (PC) and antiparallel configuration (APC).

The geometric structures of ZGNRs and PTBs are firstly optimized by the Vienna Ab initio Simulation Package[44,45]. We construct the two-probe system by composing the optimized structures to a whole system, and the optimization is performed again by the Atomistix ToolKit package till the forces on each atom is smaller than 0.01 eV/Å. The spin-dependent transport properties of the devices are studied by the Atomistix ToolKit package, which is based on the ground state spin density functional theory and the nonequilibrium Green's function method[46,47]. Although according to C. Zhang *et al.*[48], the method based on steady-state DFT would be more accurate under a bias voltage. While the difference between both methods is very small under a low bias (< 0.5 V in our calculations), so the use of methods based on ground state density functional theory though a bias voltage is used in calculations. The Perdew-Zunger parametrization of the local spin density approximation (LSDA) form of functions is employed for the exchange-correlation potential. In the calculations, the real space grid technique is used with the energy cutoff of 150 Ry as the required cutoff energy in numerical integrations. The *k*-point grid 1, 1, and 100 are used in the *x*, *y*, *z* directions, respectively, where *z* is the electron transport direction. Open boundary conditions are used to describe the electronic and transport properties of the devices. A vacuum layer of 12 Å is added to avoid the interaction between adjacent ribbons. The wave functions of all atoms are expanded by double-zeta polarized basis set. The temperature of the electrodes is set to be 300 K. The spin-polarized current through the system is calculated using the Landauer-Büttiker formula[49],

$$I_\sigma(V_b) = \frac{e}{h}\int_{\mu_R(V_b)}^{\mu_L(V_b)} \left\{ T_\sigma(E,V_b)\left[f_L(E,V_b) - f_R(E,V_b) \right] \right\} dE \qquad (1)$$

Here e is the electron charge, h is the Planck's constant, and T_σ is the transmission of an electron with spin σ. $f_{L(R)}(E,V_b)$ is the Fermi-Dirac distribution function of the left (right) electrode, and $\mu_{L(R)}(V_b)$ is the chemical potential of the

left (right) electrode, where V_b denotes the external bias voltage. T_σ can be obtained from the equation,

$$T_\sigma(E,V_b) = Tr\left[\mathrm{Im}\left\{\sum\nolimits_{L_\sigma}^{r}(E,V_b)\right\} G_\sigma^r(E,V_b) \times \mathrm{Im}\left\{\sum\nolimits_{R_\sigma}^{r}(E,V_b)\right\} G_\sigma^a(E,V_b)\right] \quad (2)$$

Here $G^r\left(G^a\right)$ is the retarded (advanced) Green's function matrix, and $\sum_L^r\left(\sum_R^r\right)$ is the retarded self-energy matrix for the left (right) electrode.

Results and discussions

We calculate the molecular energy spectrum of PTB, as shown in Fig. 2(a). The Fermi level is zero energy. The highest occupied molecular orbital (HOMO) and the lowest unoccupied molecular orbital (LUMO) is near the Fermi level. The wave functions of both HOMO and LUMO also be plotted, which can be found in Figs. 2(b) and (c). It's clear that both wave functions are symmetric with *x*-*z* plane. For 6ZGNRs unit cell, the lattice constant is 2.461 Å, and the band structure calculation indicates it is metallic at the ferromagnetic state. There are two up-spin (down-spin) subbands which are degenerated below (above) the Fermi level in the region of $2\pi/3 \le k \le \pi$, as can be seen in Fig. 2(d). The wave functions of π and π^* subbands have been presented in Figs. 2(e) and (f), respectively. From them we can find the wave function of π subband is antisymmetric and the π^* subband is symmetric with respect to the *x*-*z* plane. We also use the spin generalized gradient approximation (SGGA) of Perdew-Burke-Ernzerhof functional have a test about the molecular energy spectrum of PTB, the band structure of 6ZGNRs. For Figs. 2(a) and (d), we can see the molecular energy spectrum of PTB and the band structure of 6ZGNRs calculated by SGGA (the red line) and LSDA (the black line) are nearly the same. The only difference appears in the band of 6ZGNRs, the degenerated energy point of up-spin band at X point is changed from -0.30 to -0.53 eV, and that of the down-spin band is changed from 0.14 to 0.37 eV. And our results about the band strcture of 6ZGNR calculated by LSDA method are very agree with the previous studies[3139,50,51]. When the PTB is connected to the 6ZGNRs electrodes within the same plane (*y*-*z* plane) along its central line, as shown in Fig. 1(b), for passing through the device, these

electrons are required to have a wave function symmetric with respect to the *x*-*z* plane according to the quantum transmission theory.

The transmission spectra, density of states (DOS) for M1 and projected density of states (PDOS) for PTBs at zero bias with PC and APC have been calculated, as shown in Figs. 2(g) and (h). For the PC situation, the band structures of left and right electrode are the same, but for the up-spin and down-spin bands, there is an energy difference about 0.44 eV between the degenerated point of π and π^* subbands. Based on the matching principle, the π subbands of the left, right electrodes and center scattering region are mismatching, but the π^* subbands of them are matching. Therefore, only the electrons from the π^* subbands can pass through the device, so the up-spin transmission peak is about 0.44 eV energy lower than that of down-spin one (Fig. 2(g)), leading to a perfect spin-filtering effect around the Fermi level. When the magnetic orientation of the right electrode is changed from $+x$ to $-x$, the M1 will be in APC. We can find the band of left electrode does not change. While for the right electrode, the up-spin and down-spin bands are changed with each other, thus the similar transmission spectrums of up-spin and down-spin states can be observed, as presented in Fig. 2(h).

Interestingly, one can find there is no transmission spectrum between 0.7 and 1.0 eV for both spin in PC and APC although the wave function of left, right electrodes and center scattering region are matched. We plot the DOS for M1 and the PDOS for PTBs, which are the purple and green dashed lines shown in Figs. 2 (g) and (h). From them we can see there are DOS for M1 distribute between 0.7 and 1.0 eV, but there is no PDOS for PTBs appears from 0.7 to 1.0 eV, so there is no contribution of PTBs for the electrons to transport through the device. As a result, there is no transmission spectrum appears between 0.7 and 1.0 eV though the wave function are matching.

When the bias voltage is added on the left and right electrodes, the currents as a function of the applied bias voltage (*I*-*V* curves) can be gotten, as shown in Figs. 3(a) and (d). For M1 in PC, as shown in Fig. 3(a), the up-spin current has a linear increasing behavior when $|V_b|$ is lower than 0.2 V, and it reaches the biggest value at $|V_b|$=0.3 V, then it begins to decrease with the increasing of $|V_b|$, which indicates the

up-spin current has an NDR effect. While for the down-spin current, one can find it is almost zero over the whole bias region ([-0.5, 0.5 V]). As a result, M1 presents perfect spin-filtering effect. To have a quantitatively understanding about the spin-filtering effect, then the spin-filtering efficiency (SFE) is calculated based on the formula, $SFE = \left[\left(I_{\uparrow} - I_{\downarrow} \right) / \left(I_{\uparrow} + I_{\downarrow} \right) \right] \times 100\%$. As shown the blue line in Fig. 3(a), one can find the SFE is nearly 100% in [-0.5, 0.5 V] bias region, which indicates the M1 can be act as a perfect spin-filter. For further understanding the spin transport behavior, we plot the up-spin and down-spin transmission spectra as a function of electron energy and bias voltage, presented in Figs. 3(b) and (c). It is clear that there are up-spin transmissions spectrums come into the bias window, but there is no down-spin transmission spectrum appears in the whole bias window. As the current is determined by the integral of $T(E,V_b)$ within the bias window (*Eq*.1), so the up-spin current is much larger than that of down-spin one, leading to the perfect spin-filtering effect.

For M1 in APC, as shown in Fig. 3(d), the *I-V* curve presents semi-conductive properties with a threshold voltage of 0.1 V. It is clearly seen that the down-spin current only appears in the positive bias regions, while the up-spin current only appears in the negative bias regions, which indicates M1 has a perfect bipolar spin-filtering effect and can be used as spin-diode. The SFE is shown in Fig. 3(d) with a blue line, where one can find it is nearly 100% in bias region of [-0.5, -0.1V], and then has a spin-flip phenomenon, the SFE becomes -100% in [0.1, 0.5V]. And our calculation shows the rectifying ratio can reach 6.8×10^3. All these results show that M1 in APC is a perfect multifunctional spin electronic device. From the transmission spectra as a function of electron energy and bias voltage, as presented in Figs. 3(e) and (f), we can have a further understanding about the spin transport properties of M1 in APC. When $|V_b|$ is smaller than 0.1 V, there is no transmission spectrum appears in the bias window, so the current is almost zero. But when $|V_b|$ is larger than 0.1 V, one can find the transmission spectrum begins to come into the bias window, and increasing with $|V_b|$ increases. What's more, the up-spin transmission spectrum appears in the negative bias region, while the down-spin one appears in the positive

bias region, which is in perfect accordance with the *I-V* curves.

To explore the mechanism of the spin-filtering effect, we give the band structures of the left (right) electrode and the transport spectra of M1 at 0.3 V in PC and APC, as shown in Figs. 4(a) and (d). For M1 in PC, when a 0.3 V bias is applied, the bands of the left electrode shift downward with 0.15 eV, meanwhile the bands of the right electrode shift upward with 0.15 eV. As a result, the π and π^* subbands for both spin states of the left and right electrodes are overlapped with each other in the bias window (Fig. 4(a)). But because only the up-spin π^* of the left electrode can match with that of PTB in the scattering region and the right electrode, thus there is only up-spin transmission spectrum appears. Furthermore, we also plot the transmission pathways of up-spin and down-spin in 0.1 eV for M1 at 0.3 V in PC, presenting in Figs. 4(b) and (c), respectively. The transmission pathways T_{ij} can show us the local bond contributions to the transmission coefficient, for example, the total transmission coefficient between two parts A and B can be expressed as $T(E)=\sum_{i\in A, j\in B} T_{ij}(E)$. It can be seen the up-spin electrons can transport from the left electrode to the right electrode, and more interesting is that the transport of the electrons are mainly along the C bond in the phenyl rings instead of hopping transport in pristine ZGNRs device[51]. While the down-spin transmission pathway is localized, this indicates that the down-spin current channels are blocked.

Similar with M1 in PC, for M1 in APC, the addition of 0.3 V bias makes the bands of the left (right) electrode shift downward (upward) with 0.15 eV, as one can see in Fig. 4(d), the π and π^* subbands of both spin states appear in the bias window. Due to the mismatching of π subbands among the left (right) electrode and the PTB in the scattering region, only the down-spin transmission spectrum appears in bias window and the down-spin electrons can pass through. This can also be understood by the transmission pathway, as shown in Figs. 4(e) and (f). The transmission of up-spin electrons are completely localized in the left part, so there is no up-spin electrons pass through the device, the corresponding transmission coefficient is zero. While for the down-spin state, we can see the transmission pathway is delocalized, and the electrons

can easily transport from the left electrode to right electrode. As a result, the down-spin electrons are conductive, and a perfect spin-filtering effect can be found in M1.

The following we have a research about the effects of the rotation of PTB plane around the C chain on the electronic transport properties of the device. Fig. 5 shows the spin-dependent *I-V* curves for M2, M3 and M4 in PC and APC. For convenience of comparing, the spin-dependent *I-V* curves of M1, which are the black dashed lines in Fig. 5, have also been given. Comparing the up-spin *I-V* curves of M1-M3 in PC (Fig. 5(a)), one can find the similar transmission behavior, but the value of current is gradually decreased. When it comes to M4, the currents are nearly zero (10^{-7}μA). So, we can get the conclusion that the currents are decreased with the increasing of the angle between PTB plane and the 6ZGNRs electrodes plane. And similar phenomenon can also be found for the down-spin *I-V* curves of M1-M4 in PC (Fig. 5(b)) and the spin-dependent *I-V* curves of M1-M4 in APC (Figs. 5(c) and (d)). From above, it is clear that the devices can be realized the ON and OFF states by changing the angle between PTB plane and the 6ZGNRs electrodes plane. M1-M3 can be regarded as the ON state, while M4 can be seen as OFF state, so the proposed device can also be a perfect molecular switch. And the biggest on/off ratio is between M1 and M4 device.

Therefore, we then calculate the on/off ratio of M1/M4 in PC and APC, which can be found in Figs. 5(e) and (f), respectively. From Fig. 5(e) we can see the up-spin on/off ratios are all higher than 10^6 in the bias range of [-0.5, 0.5V], and tend to increase with the $|V_b|$ decreasing. For the on/off ratio of M1/M4 in APC, as shown in Fig. 5(f), the on/off ratio can reach to 10^7. More importantly, the on/off ratio in our device is about 10^5 orders of magnitude higher than that of former researches[52-54].

To understand the mechanism of the on/off effect in PTBs based devices, then we present the molecularly projected self-consistent Hamiltonian (MPSH) of HOMO and LUMO for up-spin states of M1-M4 at zero bias in PC, as shown in Fig. 6. For M1, M2, and M3, we can find the HOMO and LUMO are delocalized, which indicates the electrons can easily transport from the left electrode to right electrode. While for M4, one can see both the HOMO and LUMO are localized, so the transmission of

electrons between the left and right electrodes are suppressed. Additionally, comparing the HOMO and LUMO of M2, M3 and M4 with M1, it is can be found that the coupling between the alkyne triple bond and the phenyl ring of PTBs are gradually weakened. So we can get the information that, with the increasing of rotate angle of PTBs, the coupling strength between the alkyne triple bond and the phenyl ring of PTBs decreases, and nearly disappears till 90°. So the electrons can not pass through, and the on/off function can be realized.

Moreover, to further understand the current suppression behavior, we also plot the up-spin transmission spectra and up-spin local density of state (LDOS) at the Fermi level of M1-M4 in PC at 0.2 V, as shown in Fig. 7. We can see the transmission area in the bias window becoming smaller from M1 to M4, so the corresponding current also becomes smaller. Especially for M4, there is no transmission spectrum appears in the bias window, so the current is almost zero. Then we present the up-spin LDOS of M1 to M4 at the Fermi level, as shown in Figs. 7(e)-(h), it can be found the LDOS of M1 and M2 are delocalized, which offer the transmission states for electrons. For M3, though the LDOS is still delocalized, the distribution on phenyl ring becomes weaker, so the current becomes smaller. While the LDOS of M4 are completely localized in the left, right electrodes and the alkyne triple bonds (see Fig. 7(h)), so the transport channel of the electrons is blocked.

To have a further understanding about the high on/off ratio, we also consider the other conditions for the rotating of the three phenyl rings in PTB. Based on the structure of M1, we firstly rotate two of the phenyl rings of PTB from 0 to 90°, as shown in Fig. 8(a), marked as M5. Then we rotate only one of the phenyl rings from 0 to 90°, as shown in Fig. 8(b), labeled as M6. The on/off ratios of up-spin currents between the states of M1 with M5 and M6 in PC have been calculated, one can see in Fig. 8(c). For clearly comparing, we also give that of M1/M4, as shown the black line in Fig. 8(c). Obviously, the on/off ratio of M1/M5 is about 10^3, which is higher than that of M1/M6 (about 10^2), but three orders of magnitude smaller than that of M1/M4. So the M4 can effectively improve the on/off ratio. For M4, the length of perpendicular phenyl rings is 1.14 nm, and that is 0.71 nm and 0.28 nm for M5 and

M6, respectively. When the bias is applied, the probability for electrons to tunnel through the scattering region is bigger as the length of perpendicular phenyl rings decreasing, which in turn contribute to the current, thus the on/off ratio is decreased.

Conclusions

In conclusion, using the DFT and the NEGF method, we have investigated the spin-dependent electronic transport properties of the PTB connecting with two 6ZGNR electrodes. Our results show that the device has a 100% SFE and NDR effect in PC, while it has a bipolar spin-filtering effect and spin rectifying functions in APC. We also find the transport properties have a significant relationship with the angles between PTB plane and the 6ZGNRs electrodes plane. The currents are decreased with the angles increase and finally close to zero when the angle is 90°. As a result, the on/off function can be realized, and the on/off ratio is as high as 10^7. The theoretical analyses show that the matching of electronic wave functions among both 6ZGNRs electrodes and PTB scattering region, in addition with the coupling between the alkyne triple bond and the phenyl rings of PTBs are critical to the spin transport properties. These results suggest the PTB based devices have a potential utilization in designing multi-functional and high performance molecular devices.

Acknowledgements

This work is supported by the National Natural Science Foundation of China (Grant Nos. 61306149, 11274260), the Natural Science Foundation of Hunan Province (No. 14JJ3026), Hong Kong Scholars Program (No. XJ2013003), and the Research Grants Council of Hong Kong SAR (Project No. CityU 100311/11P), and the Fundamental Research Funds for the Central Universities of Central South University (No. 2015zzts014).

References

1 D. J. Frank, R. H. Dennard, E. Nowak, P. M. Solomon, Y. Taur, H. S. P. Wong, *Pro IEEE*, 2001, **89**, 259.

2 G. Maruccio, R. Cingolani, R. Rinaldi, *J. Mater Chem.*, 2004, **14**, 542.

3 M. J. Comstock, N. Levy, A. Kirakosian, J. Cho, F. Lauterwasser, J. H. Harvey, *et al.*, *Phys. Rev. Lett.*, 2007, **99**, 038301.

4 M. Urdampilleta, S. Klayatskaya, M. Ruben, W. Wernsdorfer, *ACS NANO*, 2015, **9**, 4458.

5 J. Taylor, M. Brandbyge, K. Stokbro, *Phys. Rev. B*, 2003, **68**, 121101(R).

6 X. J. Zhang, M. Q. Long, K. Q. Chen, Z. G. Shuai, Q. Wan, B. S. Zou, Y. Zhang, *Appl. Phys. Lett.,* 2009, **94,** 073503.

7 D. Zhang, M. Q. Long, X. J. Zhang, F. P. Ouyang, M. J. Li, H. Xu, *J. Appl. Phys.,* 2015, **117,** 014311.

8 J. F. Yang, L. P. Zhou, Q. Han, X. F. Wang, *J. Phys. Chem. C*, 2012, **116**, 19996.

9 X. Q. Deng, Z. H. Zhang, G. P. Tang, Z. Q. Fan, C. H. Yang, *RSC Adv.*, 2014, **4,** 58941.

10 H. Hao, X. H. Zheng, L. L. Song, R. N. Wang , Z. Zeng, *Phys. Rev. Lett.*, 2012, **108**, 017202.

11 M. Q. Long, K. Q. Chen, L. L. Wang, B. S. Zou, Z. G. Shuai, *Appl. Phys. Lett.*, 2007, **91**, 233512.

12 J. Zeng, K. Q. Chen, *J. Mater. Chem. C*, 2013, **1**, 4014.

13 Y. Zou, M. Q. Long, M. J. Li, X. J. Zhang, Q. T. Zhang, H. Xu, *RSC Adv.,* 2015, **5,** 19152.

14 X. Q. Deng, Z. H. Zhang, J. C. Zhou, G. P. Tang, *J. Appl. Phys.*, 2011, **109**, 063712.

15 C. Li, I. Pobelov, T. Wandlowski, A. Bagrets, A. Arnold, F. Evers, *J. Am. Chem. Soc.*, 2008, **130**, 318.

16 S. Guo, J. Hihath, I. Diez-Perez, N. Tao, *J. Am. Chem. Soc.*, 2011, **133**, 19189.

17 G. K. Ramachandran, T. J. Hopson, A. M. Rawlett, L. A. Nagahara, A. Primak, S. M. Lindsay, *Science*, 2003, **300**, 1413.

18 K. S. Novoselov, A. K. Geim, S.V. Morozov, D. Jiang, Y. Zhang, S. V. Dubonos, et al., *Science*, 2004, **306**, 666.

19 J. M. Cai, P. Ruffieux, R. Jaafar, M. Bieri, T. Braun, S. Blankenburg, et al., *Nature,* 2010, **466,** 470.

20 A. Basagni, F. Sedona, C. A. Pignedoli, M. Cattelan, L. Nicolas, M. Casarin, M. Sambi, *J. Am. Chem. Soc.,* 2015, **137,** 1802.

21 A. K. Geim, K. S. Novoselov, *Nat. Mater.*, 2007, **6**, 183.

22 M. Orlita, C. Faugeras, P. Plochocka, P. Neugebauer, G. Martinez, D. K. Maude, et al., *Phys. Rev. Lett.*, 2008, **101**, 267601.

23 W. Han, R. K. Kawakami, *Phys. Rev. Lett.*, 2011, **107**, 47207.

24 C. L. Kane, E. J. Mele, *Phys. Rev. Lett.,* 2005, **95,** 226801.

25 D. A. banin, S. V. Morozov, L. A. Ponomarenko, R. V. Gorbachev, A. S. Mayorov, M. I. Katsnelson, et al., *Science*, 2011, **332**, 328.

26 Z. Y. Li, H. Y. Qian, J. Wu, B. L. Gu, W. H. Duan, *Phys. Rev. Lett.*, 2008, **100**, 206802.

27 Q. M. Yan, B. Huang, J. Yu, F. Zheng, J. Zang, J. Wu, et al., *Nano Lett.*, 2007, **7**, 1469.

28 Y. W. Son, M. L. Cohen, S. G. Louie, *Phys. Rev. Lett.*, 2006, **97**, 216803.

29 C. Jin, H. Lan, L. Peng, K. Suenaga, S. Iijima, *Phys. Rev. Lett.*, 2009, **102**, 205501.

30 Y. M. Rong, J. H. Warner, *ACS NANO,* 2014, **8,** 11907.
31 Y. J. Dong, X. F. Wang, S. W. Yang, X. M. Wu, *Scientific Reports*, 2014, **4**, 6157.
32 X. Li, H. L. Li, H. Wan, G. Zhou, *Organic Electronics*, 2015, **19**, 26.
33 X. Li, H. Gao, H. Wan, H. L. Li, G. Zhou, *Chem. Phys. Lett.*, 2014, **610-611**, 298.
34 B. Cirera, Y. Q. Zhang, J. Björk, S. Klyatskaya, Z. Chen, M. Ruben, et al., *Nano Lett*., 2014, **14**, 1891.
35 F. Moresco, G. Meyer, K. H. Rieder, H. Tang, A. Gourdon, C. Joachim, *Phys. Rev. Lett*., 2001, **86**, 672.
36 C. B. Madsen, L. B. Madsen, S. S. Viftrup, M. P. Johansson, T. B. Poulsen, L. Holmegaard, et al., *Phys. Rev. Lett.*, 2009, **102**, 073007.
37 W. F. Xiang, C. K. Lee, *Appl. Phys. Lett*., 2010, **96**, 193113.
38 M. G. Vergniory, J. M. Granadino-Roldan, A. Garcia-Lekue, L. W. Wang, *Appl. Phys. Lett*., 2010, **97**, 262114.
39 W. Y. Kim, K. S. Kim, *Nature Nanotechnology*, 2008, **3**, 408.
40 W. H. Wang, K. Pi, Y. Li, Y. F. Chiang, P. Wei, J. Shi, et al., *Phys. Rev. B*, 2008, **77**, 020402(R).
41 Q. Yue, S. L. Chang, J. C. Tan, S. Q. Qin, K. Jun, J. B. Li, *Phys. Rev. B*, 2012, **86**, 235448.
42 X. Q. Deng, Z. H. Zhang, C. H. Yang, H. L. Zhu, B. Liang, *Organic Electronics*, 2013, **14**, 3240.
43 J. Zeng, K. Q. Chen, J. He, X. J. Zhang, C. Q. Sun, *J. Phys. Chem. C*, 2011, **115**, 25072.
44 G. Kresse, J. Furthmüller, *Comput. Mater. Sci.*, 1996, **6**, 15.
45 G. Kresse, J. Furthmüller, *Phys. Rev. B*, 1996, **54**, 11169.
46 J. P. Perdew, A. Zunger, *Phys. Rev. B*, 1981, **23**, 5048.
47 M. Brandbyge, J. L. Mozos, P. Ordejón, J. Taylor, K. Stokbro, *Phys. Rev. B*, 2002, **65**, 165401.
48 C. Zhang, *J. At. Mol. Sci.* 2014, **5,** 95.
49 M. Büttiker, Y. Imry, R. Landauer, S. Pinhas, *Phys. Rev. B*, 1985, **31**, 6207.
50 M. G. Zeng, L. Shen, M. Zhou, C. Zhang, and Y. P. Feng, *Phys. Rev. B,* 2011, **83**, 115427.
51 X. Q. Deng, Z. H. Zhang, G. P. Tang, Z. Q. Fan, C. H. Yang, *Carbon*, 2014, **66**, 646.
52 R. Pati, S. P. Karna, *Phys. Rev. B*, 2004, **69**, 155419.
53 T. B. Martins, A. Fazzio, A. J. R. da Silva, *Phys. Rev. B*, 2009, **79**, 115413.
54 H. Wan, B. Zhou, X. Chen, C. Q. Sun, G. Zhou, *J. Phys. Chem. C*, 2012, **116**, 2570.

Figures

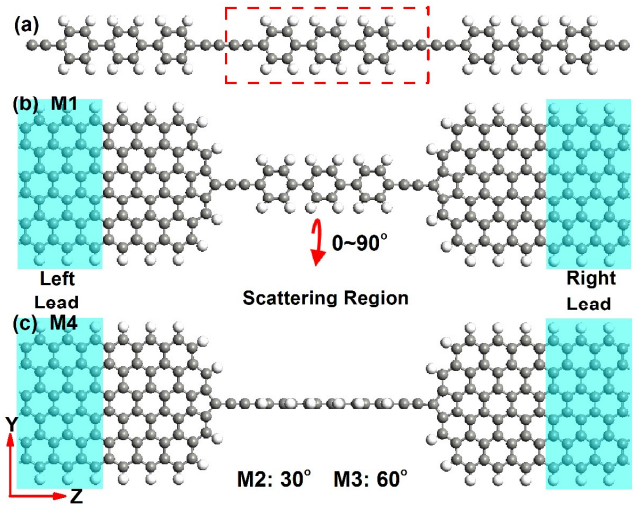

Fig. 1 (Color online) (a) The supercell of PTBs, (b) and (c) Two-probe systems of M1 and M4. The structure in the red dashed rectangle is the unit cell of PTBs. The red curved arrow gives the rotated direction of center scattering region. The gray and white balls represent C and H atoms, respectively. The blue shade areas are the electrode regions.

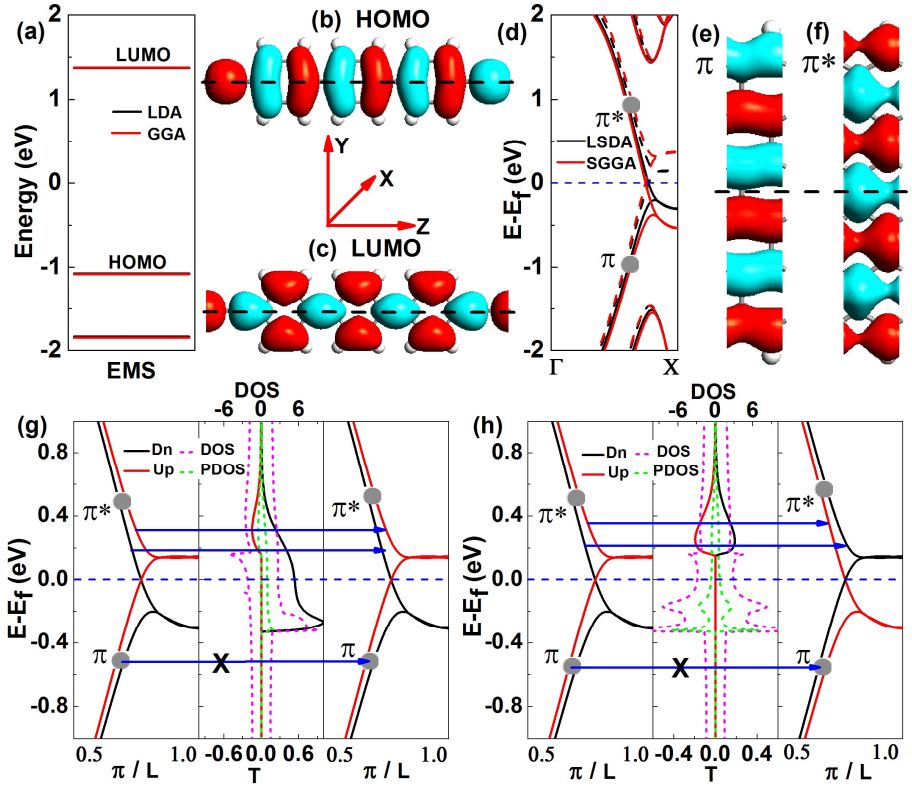

Fig. 2 (Color online) (a) The molecular energy spectrum of PTB, (b) and (c) The wave functions of HOMO and LUMO, (d) Band structure of 6ZGNRs. (e) and (f) The wave functions (for π and

π^* subbands at Γ point) of 6ZGNRs. (g) [(h)] The band structures for the left electrode (left panels), transmission spectra, DOS and PDOS (middle panels), and the band structures for the right electrode (right panels) at zero bias of M1 in PC [APC]. The blue dashed line is the Fermi level. The black dashed line indicates the *x*-*z* plane. The blue arrows and crossed arrows represent the conductive and prohibited electron transport channels.

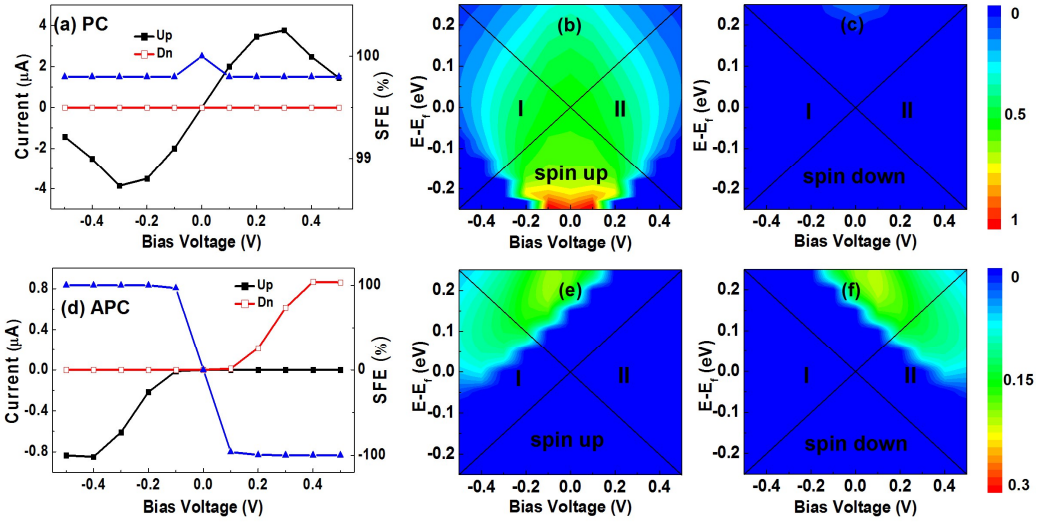

Fig. 3 (Color online) (a) [(d)] The spin-dependent *I*-*V* curves and SFEs for M1 in PC [APC]. (b) and (c) [(e) and (f)] The spin-resolved transmission spectrum as a function of electron energy and bias voltage for M1 in PC [APC]. The regions I and II between the black solid lines denote the negative and positive bias windows, respectively.

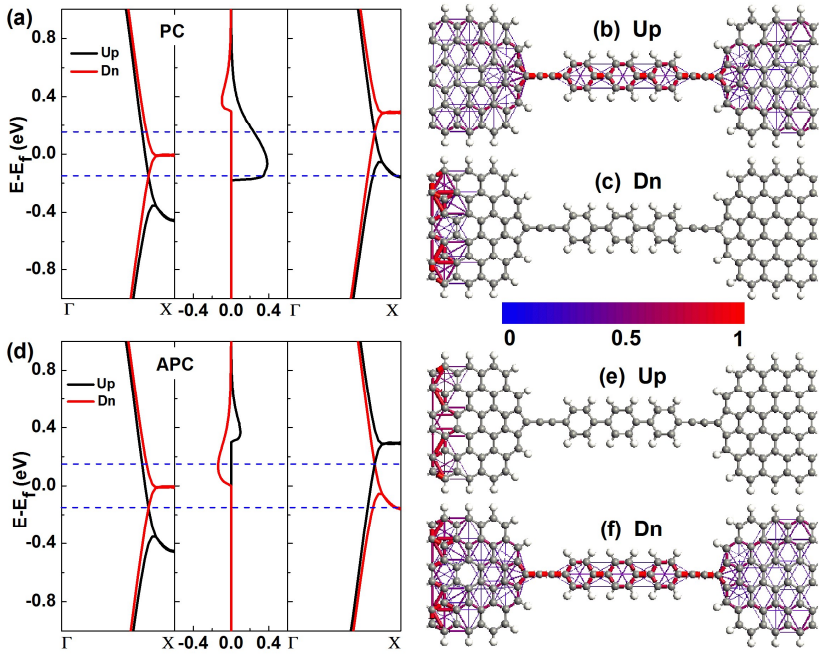

Fig. 4 (Color online) (a) [(d)] The band structures for the left electrode (left panels), transmission spectra (middle panels), and the band structures for the right electrode (right panels)

at V_b=0.3 V of M1 in PC [APC]. (b) and (c) [(e) and (f)] The up-spin and down-spin electronic transmission pathways of M1 with PC [APC] in 0.1 eV at V_b=0.3 V. The region between the blue dashed lines is the energy region contributes to the current, i.e. the bias window.

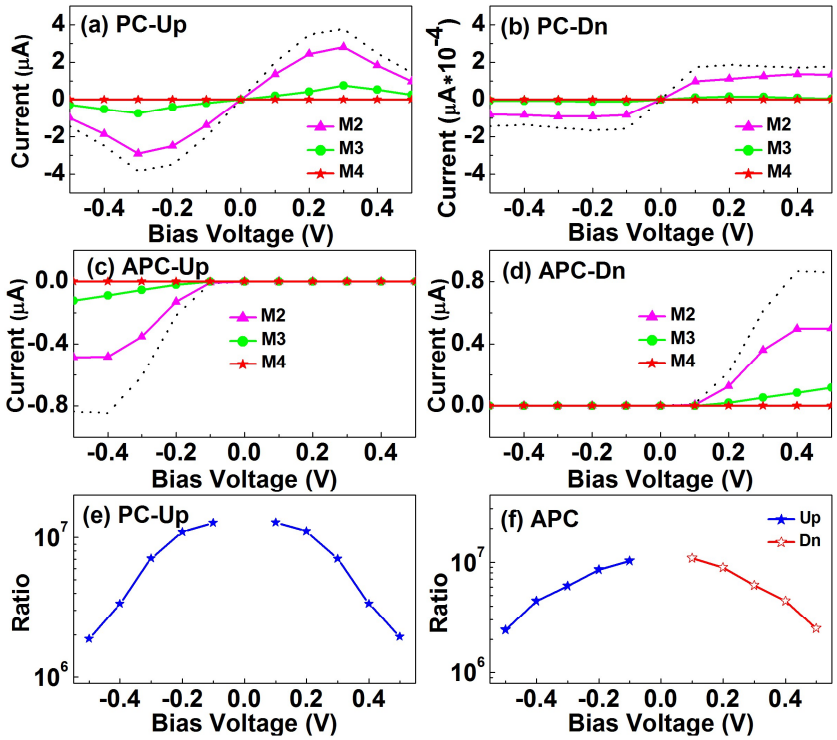

Fig. 5 (Color online) (a) and (b) [(c) and (d)] The spin-dependent *I-V* curves for M2-M4 in PC [APC]. (e) [(f)] The on/off ratio of M1/M4 in PC [APC]. The black dashed lines are the *I-V* curves of M1.

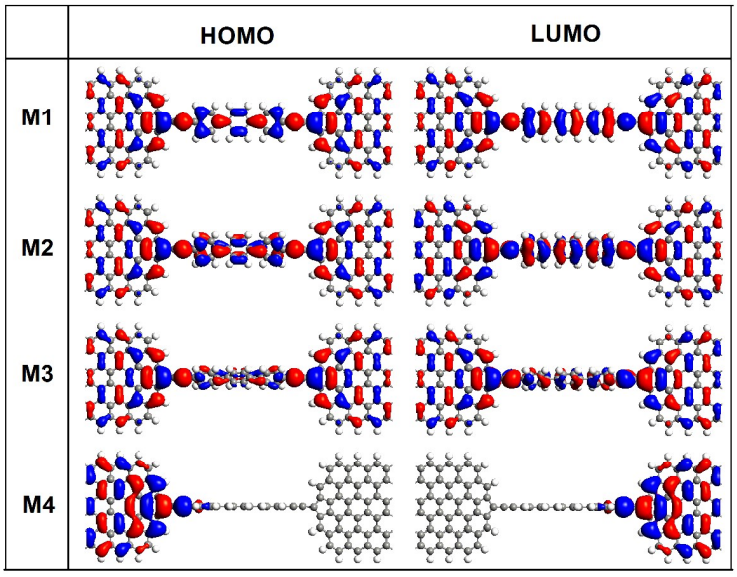

Fig. 6 (Color online) The MPSH of HOMO and LUMO for up-spin state of M1-M4 at zero bias

in PC. The red and blue colors indicate the positive and negative signs of the wave functions, respectively. The isovalue is 0.03 $Å^{-3/2}$.

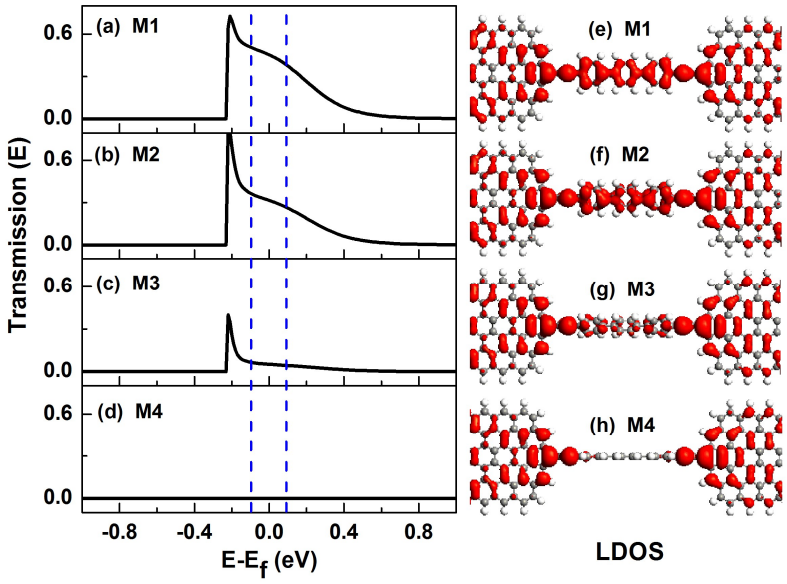

Fig. 7 (Color online) (a)-(d) The up-spin transmission spectra of M1-M4 at 0.2 V in PC. (e)-(h) The up-spin LDOS of M1-M4 at the Fermi level. The isovalue is 0.05 $Å^{-3}$. The region between the blue dashed lines is the energy region contributes to the current, i.e. the bias window.

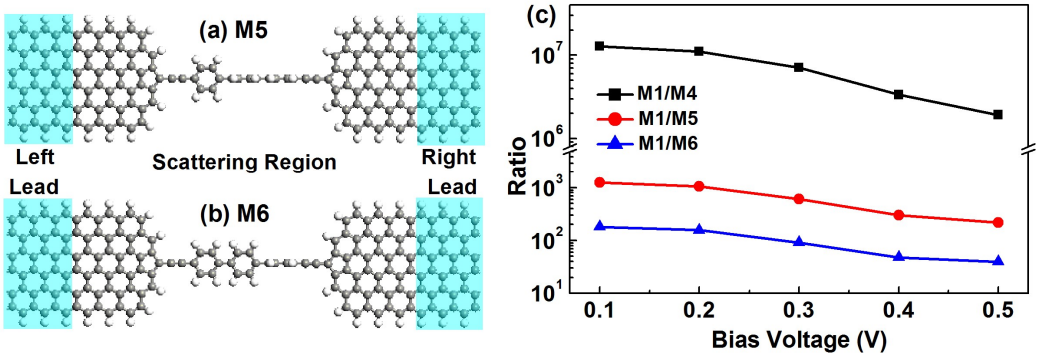

Fig. 8 (Color online) (a) and (b) Two-probe systems of M5 and M6. (c) The up-spin on/off ratio of M1/M4, M1/M5, and M1/M6 in PC, respectively.